and obtained the gamma-ray spectra of radioactive sources. The energy resolutions were 2.51 keV (FWHM) for a gamma ray of 59.5 and 2.35 keV (FWHM) for a gamma ray of 122 keV at room temperature. We are now designing a low-noise ceramic carrier to be assembled with the bare chip. In addition, a robust version of the ASIC including a leakage current compensation circuit is also being developed.

Acknowledgments

The authors would like to express their sincere gratitude for the financial support of JAXA with regards to the Steering Committee of Space Engineering.

References

[1] T. Takahashi, K. Makishima, Y. Fukazawa, M. Kokubun, K. Nakazawa, M. Nomachi, H. Tajima, M. Tashiro, Y. Terada, New Astron. Rev. 48 (2004) 269.
[2] C. Budtz-Jørgensen, T. Takahashi, L. Piro, I. Kuvvetli, A. Holland, D. Lumb, P. de Korte, Proc. SPIE 5165 (2004).
[3] T. Takahashi, et al., Nucl. Instr. and Meth. A 541 (2005) 332.
[4] T. Takahashi, S. Watanabe, IEEE Trans. Nucl. Sci. NS-48 (2001) 950.
[5] T. Takahashi, Exp. Astron. 20 (2006) 317.
[6] S.D. Kravis, T.O. Tumer, G. Visser, D.G. Maeding, S. Yin, Nucl. Instr. and Meth. A 422 (1999) 352.
[7] K. Oonuki, H. Inoue, K. Nakazawa, T. Mitani, T. Tanaka, T. Takahashi, C.M.H. Chen, W.R. Cook, F.A. Harrison, Proc. SPIE 5501 (2004) 218–227.
[8] O. Gevin, F. Lugiez, O. Limousin, P. Baron, C. Blondel, X. Coppolani, B.P.F. Dirks, E. Delagnes, Nucl. Instr. and Meth. A 567 (2006) 140.
[9] K. Tamura, T. Hiruta, H. Ikeda, H. Inoue, T. Kiyuna, Y. Kobayashi, K. Nakazawa, T. Takashima, T. Takahashi, IEEE Trans. Nucl. Sci. NS-52 (2005) 2023.
[10] T. Hiruta, K. Tamura, H. Ikeda, K. Nakazawa, T. Takasima, T. Takahashi, Nucl. Instr. and Meth. A 565 (2006) 258.
[11] H. Ikeda, Nucl. Instr. and Meth. A 569 (2006) 98.
[12] E. Beuville, K. Borer, E. Chesi, E.H.M. Heijne, P. Jarron, B. Lisowski, S. Singh, Nucl. Instr. and Meth. A 288 (1990) 157.
[13] O. Toker, S. Masciocchi, E. Nygård, A. Rudge, P. Weilhammer, Nucl. Instr. and Meth. A 340 (1994) 572.
[14] E. Nygård, P. Aspell, P. Jarron, P. Weilhammer, K. Yoshioka, Nucl. Instr. and Meth. A 301 (1991) 506.
[15] P. Aspell, R. Boulter, A. Czermak, P. Jalocha, P. Jarron, A. Kjensmo, W. Lange, E. Nygård, A. Rudge, O. Toker, M. Turala, H. Von Der Lippe, U. Walz, P. Weilhammer, K. Yoshioka, Nucl. Instr. and Meth. A 315 (1992) 425.
[16] O. Toker, S. Masciocchi, E. Nygård, A. Rudge, P. Weilhammer, Nucl. Instr. and Meth. A 340 (1994) 572.
[17] G.D. Geronimo, P. O'Connor, J. Grosholz, IEEE Trans. Nucl. Sci. NS-47 (2000) 1857.
[18] W.R. Cook, J.A. Burnham, F.A. Harrison, Proc. SPIE 3445 (1998) 347.
[19] H. Spieler, Semiconductor Detector Systems, Oxford University Press, Oxford, 2005, pp. 145–148.
[20] T. Takahashi, T. Mitani, Y. Kobayashi, M. Kouda, G. Sato, S. Watanabe, K. Nakazawa, Y. Okada, M. Funaki, R. Ohno, K. Mori, IEEE Trans. Nucl. Sci. NS-49 (2002) 1297.
[21] K. Nakazawa, T. Takahashi, S. Watanabe, G. Sato, M. Kouda, Y. Okada, T. Mitani, Y. Kobayashi, Y. Kuroda, M. Onishi, R. Ohno, H. Kitajima, Nucl. Instr. and Meth. A 512 (2003) 412.

Available online at www.sciencedirect.com
ScienceDirect
Nuclear Instruments and Methods in Physics Research A 579 (2007) 859–865
NUCLEAR INSTRUMENTS & METHODS IN PHYSICS RESEARCH Section A
www.elsevier.com/locate/nima

Development of double-sided silicon strip detectors (DSSD) for a Compton telescope

Shin'ichiro Takeda[a,b,*], Shin Watanabe[a], Takaaki Tanaka[a,b], Kazuhiro Nakazawa[a], Tadayuki Takahashi[a,b], Yasushi Fukazawa[c], Hajimu Yasuda[c], Hiroyasu Tajima[d], Yoshikatsu Kuroda[e], Mitsunobu Onishi[e], Kei Genba[e]

[a]*Institute of Space and Astronautical Science, 3-1-1, Yoshinodai, Sagamihara 229-8510, Japan*
[b]*University of Tokyo, 7-3-1, Hongo, Bunkyo, Tokyo 113-0033, Japan*
[c]*Hiroshima University, Higashi-Hiroshima 739-8526, Japan*
[d]*Stanford Linear Accelerator Center, Stanford, CA 94309-4349, USA*
[e]*Nagoya Guidance and Propulsion System Works, Mitsubishi Heavy Industries, Ltd., Komaki, Aichi 485-8561, Japan*

Available online 31 May 2007

Abstract

The low noise double-sided silicon strip detector (DSSD) technology is used to construct a next generation Compton telescope which is required to have both high-energy resolution and high-Compton reconstruction efficiency. In this paper, we present the result of a newly designed stacked DSSD module with high-energy resolution in highly packed mechanical structure. The system is designed to obtain good P-side and N-side noise performance by means of DC-coupled read-out. Since there are no decoupling capacitors in front-end electronics before the read-out ASICs, a high density stacked module with a pitch of 2 mm can be constructed. By using a prototype with four-layer of DSSDs with an area of 2.56 cm × 2.56 cm, we have succeeded to operate the system. The energy resolution at 59.5 keV is measured to be 1.6 keV (FWHM) for the P-side and 2.8 keV (FWHM) for the N-side, respectively. In addition to the DSSD used in the prototype, a 4 cm wide DSSD with a thickness of 300 μm is also developed. With this device, an energy resolution of 1.5 keV (FWHM) was obtained. A method to model the detector energy response to properly handle split events is also discussed.

PACS: 07.85.–m; 95.55.Ka

Keywords: Silicon strip detector; Compton telescope; Gamma-ray astronomy

1. Introduction

The observation of high-energy astrophysical phenomenon utilizing sub-MeV/MeV gamma rays is an attractive result that opens up a new window for studying particle acceleration and nucleon synthesis in the universe. However, the sensitivity is limited because of high background, low efficiency, and the difficulty of imaging utilizing focussing technology. As demonstrated by COMPTEL [1] onboard CGRO (Compton Gamma-Ray Observatory), in the range from ~1 to several tens of MeV, a significant reduction of background by means of reconstructing Compton scattering is proved to be useful in this difficult spectral band.

Our approach is to apply the concept of Compton telescope in the range of several 10 keV to several 100 keV. In order to extend the capability down to low energy gamma rays, the use of a stack of double-sided silicon strip detectors (DSSD) [2] is very attractive. Taking advantage of significant progress in technology related to Si and CdTe imaging detecors, we are developing a new generation of Compton telescope, the semiconductor Compton telescope (Si/CdTe Compton telescope) [3–8]. Si works as a good scattering medium because the cross-section of Compton scattering becomes larger than that of photo-absorption above 50 keV. In addition, the advantage of Si is its

*Corresponding author. Institute of Space and Astronautical Science, 3-1-1, Yoshinodai, Sagamihara 229-8510, Japan.
E-mail address: takeda@astro.isas.jaxa.jp (S. Takeda).

0168-9002/$ - see front matter © 2007 Published by Elsevier B.V.
doi:10.1016/j.nima.2007.05.305

relatively small Doppler broadening effect [9] compared with Ge or CdTe [10]. On the other hand, CdTe works very nicely as an absorber thanks to its high atomic number and high density.

The scattering part is very important in the Compton telescope. In order to cover an energy range from several 10 keV, the energy threshold of the detector must be low, because the energy of recoil electrons is almost below 10 keV in this energy band. Furthermore, a high Compton scattering probability is desirable to obtain a high efficiency as a Compton telescope. In the Si/CdTe Compton telescope, we employ a DSSD module that consists of compactly stacked layers of DSSDs (Fig. 1). In order to be hermetically and symmetrically enclosed by absorbers, the scattering part needs to have a compact structure. Also, a symmetrical structure is desirable to reduce possible systematic errors in measurements of linear polarization of gamma rays.

In order to demonstrate the concept of the Si/CdTe Compton telescope, we have developed high-quality DSSD together with a low noise analog ASIC to realize a noise level as low as 1–2 keV (FWHM) [11,12]. As a next step, we work on improving the Compton scattering efficiency. The development of a large volume and high-density DSSD module is a key to achieve the requirements. In addition, the mass of the supporting materials including the read-out electronics should be minimized to reduce the interaction of scattered photons with inactive materials. The improvement of the N-side energy resolution also increases the efficiency. In a previous prototype, an energy resolution of 1.3 keV (FWHM) on the P-side is achieved, while 3.8 keV on the N-side. Thus, an improved N-side resolution makes it possible to determine the position of Compton scattering with high accuracy for smaller energy deposits.

In this paper, we present the results of the new prototype of stacked DSSD module which emphasizes energy resolution and density in Section 2. Next, the results from a 4 cm wide DSSD which improves the Compton scattering efficiency is reported in Section 3. Finally, a detailed DSSD energy response including inter-strip events is discussed in Section 4.

2. Prototype of high density stacked DSSD module

2.1. The new DSSD board

The DSSD used here is the 2.56 cm wide device developed with Hamamatsu Photonics, Japan. See Tajima et al. [12] for the details of this device. The device was produced from an n-type wafer which has resistivity of 5 kΩ cm. The wafer thickness is 300 μm. The N-side has a floating p-implantation between strips to isolate adjacent strips. The strip pitch is 400 μm and the width is 300 μm on each side. The Al electrodes are DC-coupled on each implantation.

A photograph of the newly developed DSSD board is shown in Fig. 2. It consists of one DSSD and two specially designed low noise analog VLSI, VA64TAs, mounted on a small circuit board. The VA64TA is manufactured by IDEAS ASA, Norway in collaboration with us. It has a 64 channel input and can be used for both positive and negative input charges. Combined with the compact design, the support structure is made of plastic instead of Al_2O_3 ceramic. The average thickness of the support in the horizontal direction is 1.4 g/cm^2.

A DC-coupled read-out is employed not only on the P-side but also on the N-side to obtain good energy resolution. To apply reverse voltage, the N-side circuit as a whole is biased by 100 V. The decoupling is performed in the read-out system as described later. Since this system does not need decoupling capacitors in front-end, it becomes possible to shorten the stack pitch to 2 mm from 6 mm in a previous prototype [5,6].

2.2. Four-layer stacked DSSD module

Combining the new DSSD board, a four-layer stack of the DSSD module is constructed. Fig. 3 shows the

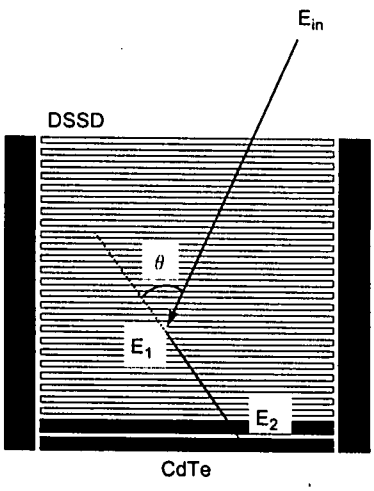

Fig. 1. Design of stacked DSSD module with CdTe detectors (absorbers).

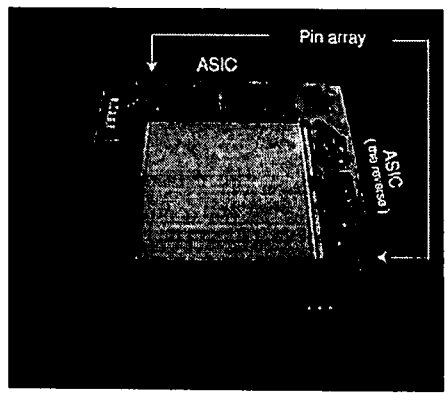

Fig. 2. Photograph of a DSSD board.

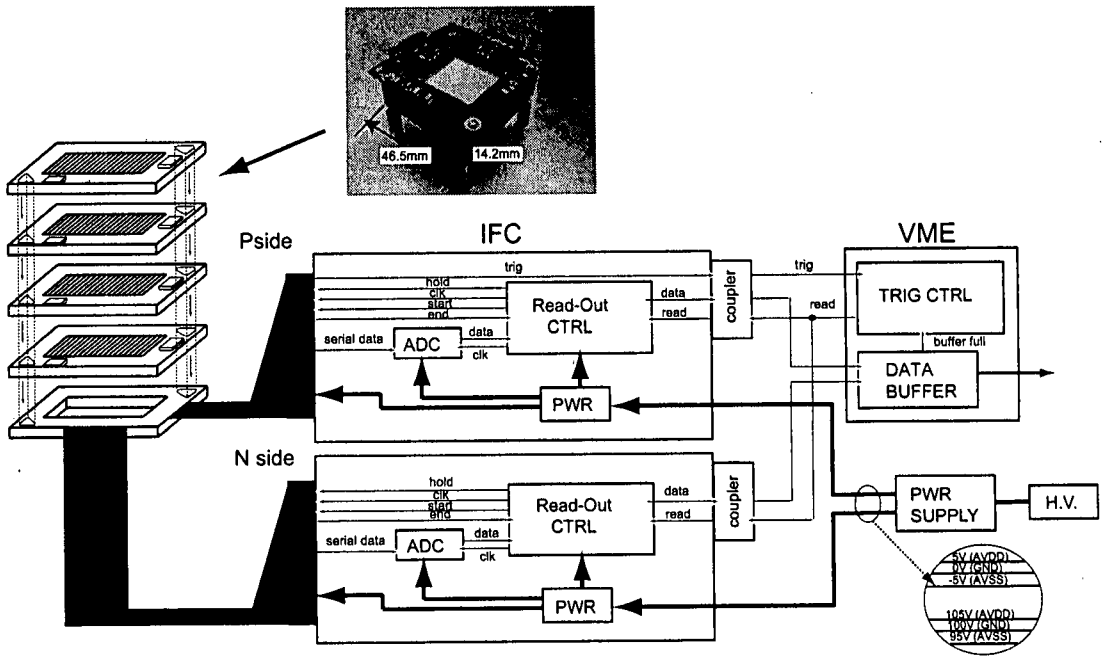

Fig. 3. Schematic diagram of the four-layer stacked DSSD module.

schematic diagram of the system. Four DSSD boards are daisy-chained via pin arrays and stacked with a 2 mm pitch. Each side has the same read-out board, the Inter Face Card (IFC), which controls the read-out sequence. The IFC interchanges the digital signal with the external system via an ultra fast coupler with 2000 V tolerance, hence we can supply the reverse bias to each DSSD by means of operating two IFCs under voltage gap corresponding to reverse bias. Consequently, we can realize DC-coupled read-out on both sides.

All layers were successfully operated at −20 °C and a bias of 100 V. In Fig. 4, we present sum spectra of both the P-side and N-side in each layer. The energy resolution at 59.5 keV is obtained to be 1.6 keV (FWHM) in P-side, which is about 0.3 keV larger than the expected value calculated from VA64TA noise performance and the input capacitance of DSSD. The difference is explained by the pitch adapter capacitance between the DSSD and LSI since we observed 1.2 keV (FWHM) for the channels with a short pitch adapter. We are currently fabricating a new LSI with optimized input channel pitch to minimize the length of the pitch adaptor.

In spite of the effect of the pitch adapter capacitance, we recognize an improvement of the N-side energy resolution from 3.8 to 2.8 keV (Fig. 4 right), compared with AC-coupled read-out with RC-bias chip [11] with $R \simeq 4\,\mathrm{G\Omega}$ and $C \simeq 50\,\mathrm{pF}$ in the previous prototype [5,6]. The noise on the N-side is still larger than what was expected from the LSI performance and the total capacitance load. The origin of this "excess noise" is under investigation.

3. A 4 cm wide DSSD

Another way to increase the efficiency is to enlarge the DSSD itself. We have developed a 4 cm wide DSSD for the future stacked DSSD module. Although the preliminary results are already summarized by Nakazawa et al. [13], we here present the detailed performance of the device including energy response. The strip length is 3.84 cm and thus the effective area (active area × thickness) is 2.25 times larger than the 2.56 cm wide DSSD. The strip parameters are the same to these of the 2.56 cm wide DSSD. The thickness is 300 μm, while the strip pitch is 400 μm and the width is 300 μm on both sides.

3.1. Basic characteristics of the device

We measured the leakage current of two selected strips in the P-side using a KEITHLEY 237 multimeter. The I–V curve of the 4 cm DSSD with various temperatures and bias voltages is presented Fig. 5 (left). The leakage current at 100 V bias is 650 pA at 20 °C and 26 pA at −10 °C. These values are about 1.6 times larger than a 2.56 cm wide DSSD, proportional to the size of the device.

A DSSD capacitance has two origins: the body capacitance and the inter strip capacitance. We measured these capacitances using a HP4284A multimeter. The result is shown in Fig. 5 (right). The body capacitance per strip becomes constant at a value of 5 pF above a bias of 70 V. This means that the full depletion voltage is 70 V. However, the N-side inter strip capacitance still decreases even above 70 V and becomes constant around 100 V. This fact

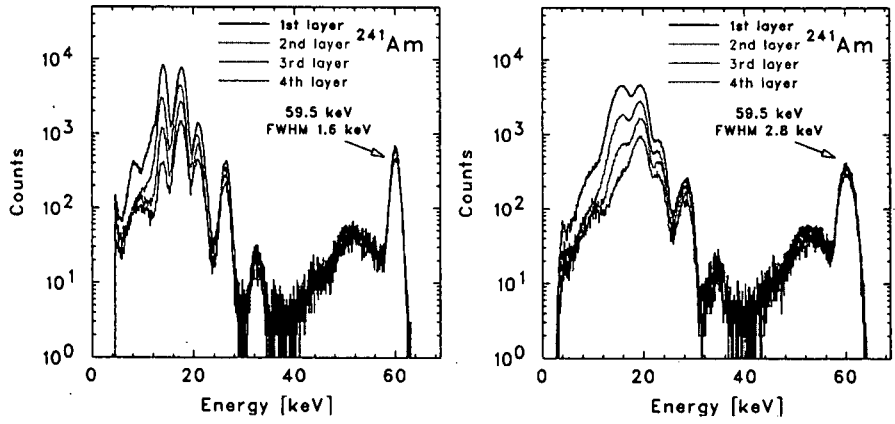

Fig. 4. Sum spectra for each layer (left: P-side, right: N-side).

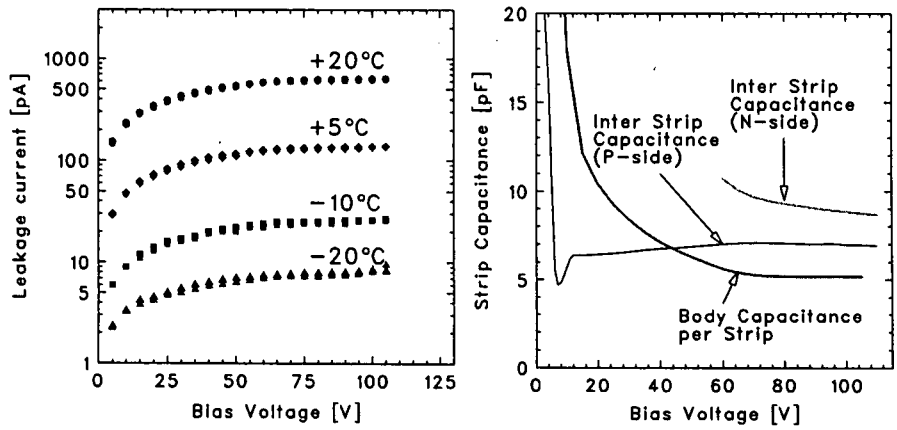

Fig. 5. Measured basic property of 4 cm wide DSSD. *I–V* curve with various temperature (left), *C–V* curve (right).

suggests that actually a 100 V bias is required to make the N-side inter strip fully isolated. Since total input capacitance is a sum of the body capacitance and the inter strip capacitance, we can estimate it as 12.2 and 14.2 pF at the P-side and N-side, respectively.

3.2. Imaging and spectroscopy

We read out the 4 cm wide DSSD using another analog LSI, VA32TA [12]. The 4 cm wide DSSD has a total of 192 channels, so we need 6 VA32TA chips. In this experiment, we apply reverse bias via a RC-bias chip on the N-side.

The DSSD was operated at −10 °C with a 100 V bias. The left panel of Fig. 6 is ^{133}Ba line image integrated in the energy band from 20 to 40 keV. The classic style car mask, made of 0.3 mm thick brass, was mounted 3 mm above the DSSD. The right panel of Fig. 6 is the sum spectra of all 96 strips in the P-side. The energy resolution at 59.5 keV is measured to be 1.5 keV (FWHM). This energy resolution is consistent with the value which is calculated from the VA32TA noise performance and input capacitance.

3.3. Pulse height correlation

We irradiated two adjacent P-side strips (Nos. 73 and 74) with 59.5 keV gamma rays from ^{241}Am. Since the attenuation length is 1.34 cm [14] for 60 keV photons, interactions occur almost uniformly in the 300 μm thickness. Fig. 7 is the distribution of the pulse height correlation. The regions surrounded by rectangles with oblique lines are lower energy lines of ^{241}Am. The distribution shows that our DSSD has roughly 10% split events which share signals between adjacent strips.

The striking feature of the plot is the opposite polarity events which are of unknown origin. This phenomenon is not detected in the same diagram generated for N-side. Because of the threshold of our measurement, we can predict that some events are undetected even though they actually interact in the DSSD. Thus there are "dead events" in the DSSD. The phenomenon is not only observed in a 4 cm wide DSSD but also in a 2.56 cm wide DSSD. The 4 cm DSSD has statistical advantage because of its larger effective area, thus it is suitable for a detailed investigation of energy response.

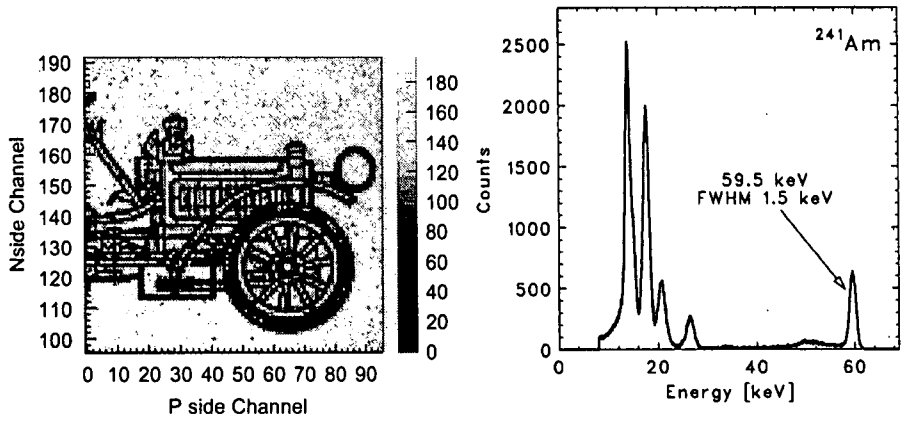

Fig. 6. A shadow image ranging from 20 to 40 keV X-ray irradiated ^{133}Ba (left), a sum spectrum of P-side irradiated ^{241}Am (right).

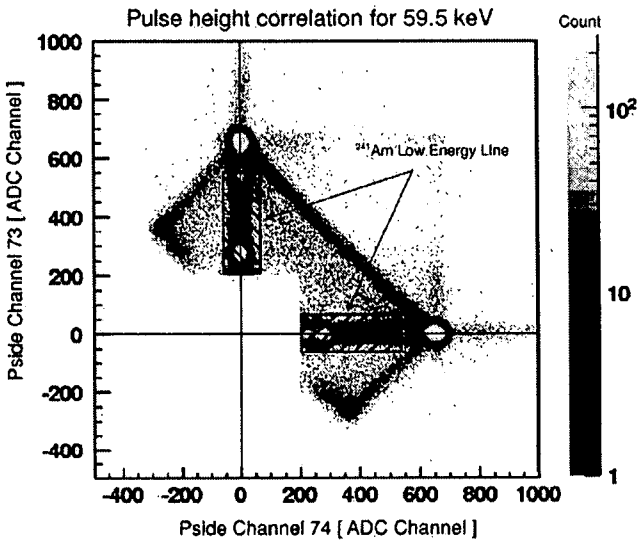

Fig. 7. Pulse height correlation between strip Nos. 73 and 74.

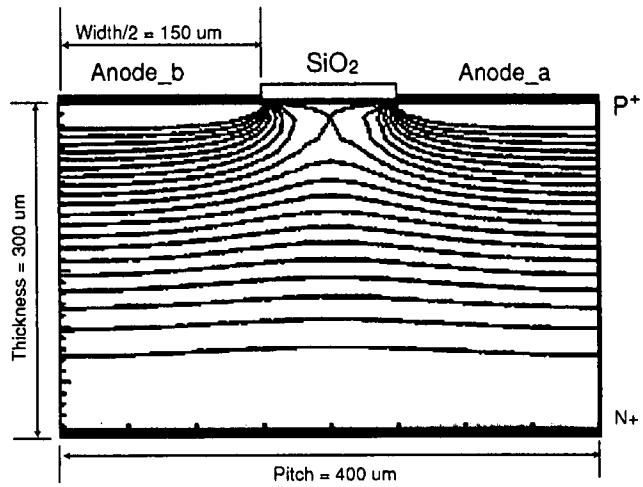

Fig. 8. Internal potential of DSSD under full depletion voltage.

Since the effect will not be negligible in Compton reconstruction, we should identify the origin of these events and evaluate the percentage of the "dead events". In the next section, we discuss these phenomenon, based on two-dimensional device simulator and the assumption of a simple charge induced model.

4. Detailed energy response of DSSD

4.1. Potential simulation

As the first step, the internal potential of the DSSD was calculated using the two-dimensional device simulator VENUS-2D, developed by Fuji Research Institute Corporation, Japan. The geometry is a cross-section perpendicular to the p-strip. We estimate the donor density of n-bulk silicon as $8.3 \times 10^{11}\,\mathrm{cm}^{-3}$ from our DSSD's resistivity and set p^+ and n^+ dope density as a typical value $1.0 \times 10^{18}\,\mathrm{cm}^{-3}$. Additionally, we set the positive fixed oxide surface charges in the Si–SiO_2 transition region to have a typical value $1.0 \times 10^{12}\,\mathrm{e/cm}^2$ [15]. This geometry fully depletes on bias voltage around 60 V, the value of which is consistent with the actual measurements (Section 3.1).

Fig. 8 is a simulated internal potential under full depletion voltage. Positive fixed oxide surface charges induce local minimum potential between the p-strips and in this region electrons are conducted to the center of SiO_2 layer, not to N-side. The local minimum potential region extends to about $1500\,\mu\mathrm{m}^2$ under SiO_2 layer.

4.2. Simulated pulse height correlation

Based on the potential simulation, we next calculated the pulse height correlation between the two anodes (Anode_a and Anode_b in Fig. 8) for 59.5 keV photo-absorption events. To estimate the charge collection, we introduce simple assumptions as follows:

(1) Holes and electrons are fully conducted either to electrodes or to the SiO_2 layers.

(2) The trajectory of a charge is simply defined by the potential taking no account of initial momentum and thermal diffusion.
(3) Electrons ($-Q$) conducted to SiO_2 induce the same amount of signal ($+\frac{1}{2}Q$) to the adjacent strips (Anode_a, Anode_b) (see Yorkston et al. [16] for experimental evidence).
(4) The initial charge cloud size is defined as $C_{init} \simeq 0.0171 \times T_e^{1.75}$ (μm) [17], where, C_{init} is the 2 sigma cloud diameter and T_e is the initial electron kinetic energy. For example, $C_{init} = 21$ μm for 59.5 keV photon absorption.

Fig. 9 is the result of the simulated pulse height correlation. The distribution (Fig. 9 top) is like an oblique rectangle which has the apex $(q,0)$, $(\frac{1}{2}q, -\frac{1}{2}q)$, $(-\frac{1}{2}q, \frac{1}{2}q)$, $(0,q)$. This corresponds to the experiment (Section 3.3). The reason of forming this distribution is because the amount of charge collection to Anode_a and Anode_b varies according to the point where the initial cloud is generated. We can roughly divide the internal region into eight sections as indicated in Fig. 9 bottom, A–G. All holes move to the nearest strip and all electrons move to N-side in A $(q,0)$ and G $(0,q)$. All holes move to the nearest strip and electrons are shared between SiO_2 and N-side in B (between $(q,0)$ and $(\frac{1}{2}q, -\frac{1}{2}q)$) and F (between $(-\frac{1}{2}q, \frac{1}{2}q)$ and $(0,q)$). All holes move to the nearest strip and all electrons move to SiO_2 in C $(\frac{1}{2}q, -\frac{1}{2}q)$ and E $(-\frac{1}{2}q, \frac{1}{2}q)$. Holes are shared between strips and all electrons move to SiO_2 in D (between $(\frac{1}{2}q, -\frac{1}{2}q)$ and $(-\frac{1}{2}q, \frac{1}{2}q)$). Holes are shared between strips and all electrons move to N-side in H (between $(0,q)$ and $(q,0)$).

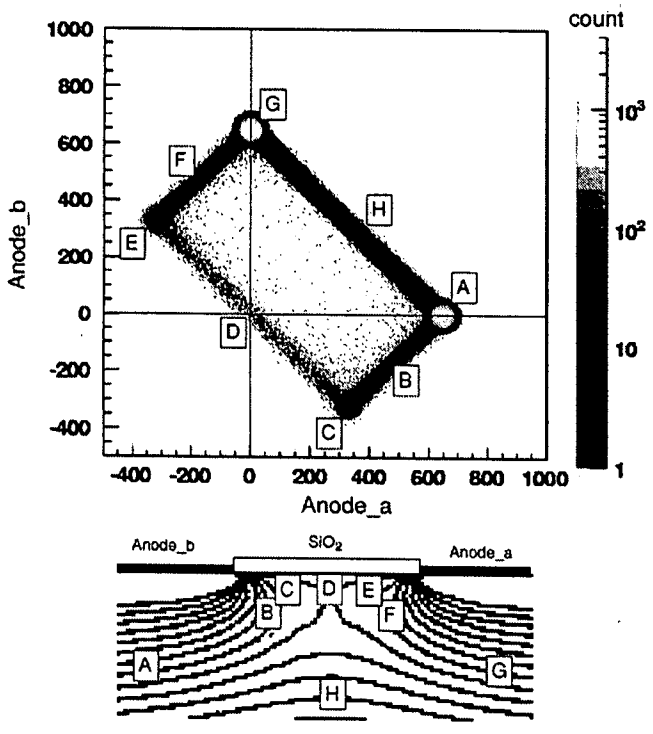

Fig. 9. Simulated pulse height correlation between adjacent strips. According to the region where initial cloud is generated, the distribution becomes oblique rectangle.

Table 1
Comparison between actual experimental data (Fig. 7) and simulation results (Fig. 9)

Region	Number of events (normalized)	
	Experiment	Simulation
A+G	100	100
H	6.3	4.1
(B+C)+(E+F)	4.5	2.0
D	N/A	0.08

Regions A to H are indicated in Fig. 9. Number of events are normalized to those in the A+G region, which is set to 100.

Table 1 shows a comparison of event distributions between experiment (Fig. 7) and simulations (Fig. 9, top). Simulations reproduce the experimental data well. In Section 3.3, we reported on the presence of "dead events". They are shown to originated from the region D (Fig. 9, bottom). In experimental data (Fig. 7), the density of these events is slightly higher than those of the simulation. This is well explained as a contribution of gamma rays below 59.5 keV, such as backscatter events around 48.3 keV (Fig. 7). Although the threshold of measurement and mixed response for different energy photons in the diagram of pulse height correlation make it difficult to measure the probability of "dead events", we predict from simulation that their probability is on the order of 0.1%.

5. Summary and future prospects

Successful operation of the four-layer stack of a DSSD module with a stack pitch of 2 mm is demonstrated. The DC-coupled read-out is employed on both the P-side and the N-side. The energy resolution of 1.6 keV (FWHM) on P-side and 2.8 keV on N-side is measured for 59.5 keV X-ray at a temperature of −20 °C. The satisfactory performance of the 4 cm wide DSSD which has 2.25 times larger effective area than a 2.56 cm wide DSSD is also demonstrated.

The presence of "dead events" is found from the diagram of pulse height correlation for 59.5 keV incident photons. A two-dimensional device simulation with simple assumptions on charge collection can reproduce the energy response observed in the data well. We conclude from the simulation that the fraction of "dead events" is on the order of 0.1%, originating from the region of the local potential minimum under the SiO_2 layer.

Further approaches for a next revision of the stacked DSSD module include a new circuit board with shorter pitch adapter and an ASIC with an optimized input pitch and on-chip digitizer. As for the detector development, tests of DSSDs with a thickness of 500 μm and size of 4 and 2.56 cm are under progress. We also plan to fabricate a 5.12 cm^2 DSSD with a thickness of 500 μm to achieve 2.5 times larger effective area than a 4 cm wide DSSD

with a thickness of 300 μm without increasing the strip capacitance.

References

[1] V. Schoenfelder, et al., Astrophys. J. Suppl. Ser. 86 (1993) 657.
[2] T. Kamae, R. Enomoto, N. Honda, Nucl. Instr. and Meth. A 260 (1987) 254.
[3] T. Takahashi, K. Nakazawa, T. Kamae, H. Tajima, Y. Fukazawa, M. Nomachi, M. Kokubun, in: Proceedings of SPIE—International Society for Optical Engineering, vol. 4851, 2003, pp. 1228–1235.
[4] T. Mitani, et al., IEEE Trans. Nucl. Sci. NS-51 (5) (2004) 2432.
[5] T. Tanaka, S. Watanabe, S. Takeda, K. Oonuki, T. Mitani, K. Nakazawa, T. Takashima, T. Takahashi, H. Tajima, N. Sawamoto, Y. Fukazawa, M. Nomachi, Nucl. Instr. and Meth. A. 568 (2006) 375.
[6] S. Watanabe, T. Tanaka, K. Nakazawa, T. Mitani, K. Oonuki, T. Takahashi, T. Takashima, H. Tajima, Y. Fukazawa, M. Nomachi, S. Kubo, M, Onishi, Y. Kuroda, IEEE Trans. Nucl. Sci. NS-52 (5) (2005) 2045.
[7] S. Watanabe, S. Takeda, S. Ishikawa, H. Odaka, M. Ushio, T. Tanaka, K. Nakazawa, T. Takahashi, H. Tajima, Y. Fukazawa, Y. Kuroda, M. Onishi, Nucl. Instr. and Meth. A 2007, in press.
[8] H. Odaka, S. Takeda, S. Watanabe, S. Ishikawa, M. Ushio, T. Tanaka, K. Nakazawa, T. Takahashi, H. Tajima, Y. Fukazawa, Nucl. Instr. and Meth. A, 2007, in press.
[9] R. Ribberfors, Phys. Rev. B 12 (1975) 2067.
[10] A. Zoglauer, G. Kanbach, in: Proceedings of SPIE—International Society for Optical Engineering, vol. 4851, 2003, pp. 1302–1309.
[11] Y. Fukazawa, T. Nakamoto, N. Sawamoto, S. Uno, T. Ohsugi, H. Tajima, T. Takahashi, T. Mitani, K. Nakazawa, in: Proceedings of SPIE—International Society for Optical Engineering, vol. 5501, 2004.
[12] H. Tajima, T. Kamae, S. Uno, T.Nakamoto, Y. Fukazawa, T. Mitani, T. Takahashi, K. Nakazawa, Y. Okada, M. Nomachi, in: Proceedings of SPIE—International Society for Optical Engineering, vol. 4851, 2003, pp. 875–884.
[13] K. Nakazawa, S. Takeda, T. Tanaka, T. Takahashi, S. Watanabe, Y. Fukazawa, N. Sawamoto, H. Tajima, T. Itoh, M. Kokubun, Nucl. Instr. and Meth. A 573 (2007) 44.
[14] See (http://physics.nist.gov/PhysRefData/Xcom/Text/XCOM.html).
[15] S. Seidel, Nucl. Instr. and Meth. A 465 (2001) 267.
[16] J. Yorkston, A.C. Shotter, D.B. Syme, G. Huxtable, Nucl. Instr. and Meth. A. 262 (1987) 353.
[17] J. Janesick et al. SPIE, X-Ray Instrumentation in Astronomy, vol. 597, 1985, pp. 364–380.

Available online at www.sciencedirect.com
ScienceDirect
ELSEVIER
Nuclear Instruments and Methods in Physics Research A 579 (2007) 871–877
NUCLEAR INSTRUMENTS & METHODS IN PHYSICS RESEARCH Section A
www.elsevier.com/locate/nima

Development of semiconductor imaging detectors for a Si/CdTe Compton camera

Shin Watanabe[a,*], Shin'ichiro Takeda[a,b], Shin-nosuke Ishikawa[a,b], Hirokazu Odaka[a,b], Masayoshi Ushio[a,b], Takaaki Tanaka[a,b], Kazuhiro Nakazawa[a], Tadayuki Takahashi[a,b], Hiroyasu Tajima[c], Yasushi Fukazawa[d], Yoshikatsu Kuroda[e], Mitsunobu Onishi[e]

[a]*Institute of Space and Astronautical Science, Japan Aerospace Exploration Agency, 3-1-1 Yoshinodai, Sagamihara, Kanagawa 229-8510, Japan*
[b]*Department of Physics, The University of Tokyo, Bunkyo, Tokyo 113-0033, Japan*
[c]*Stanford Linear Accelerator Center, Menlo Park, CA, USA*
[d]*Department of Physics, Hiroshima University, Higashi Hiroshima, Hiroshima, Japan*
[e]*Nagoya Guidance and Propulsion System Works, Mitsubishi Heavy Industries, Ltd., Komaki, Aichi 485-8561, Japan*

Available online 31 May 2007

Abstract

Si and CdTe semiconductor imaging detectors have been developed for use in a Si/CdTe Compton camera. Based on a previous study using the first prototype of a Si/CdTe Compton camera, new detector modules have been designed to upgrade the performance of the Compton camera. As the scatter detector of the Compton camera, a stack of double-sided Si strip detector (DSSD) modules, which has four layers with a stack pitch of 2 mm, was constructed. By using the stack DSSDs, an energy resolution of 1.5 keV (FWHM) was achieved. For the absorber detector, the CdTe pixel detector modules were built and a CdTe pixel detector stack using these modules was also constructed. A high energy resolution ($\Delta E/E \sim 1\%$) was achieved. The improvement of the detection efficiency by stacking the modules has been confirmed by tests of the CdTe stack. Additionally, a large area CdTe imager is introduced as one application of the CdTe pixel detector module.

PACS: 95.55.Ka; 29.40.Wk

Keywords: Gamma-ray detector; Compton telescope; Silicon strip detector; Cadmium telluride (CdTe)

1. Introduction

The Compton camera is the most promising approach for gamma-ray imaging and spectroscopy in the range of several tens keV to several MeV. For Compton cameras, both good energy resolution and good position resolution are very important to achieve a Compton reconstruction that has high levels of accuracy. We propose a new concept of the Si/CdTe semiconductor Compton cameras based on our developments of Si and CdTe semiconductor imaging detectors [1,2].

The basic concept of the Si/CdTe Compton camera is shown in Fig. 1. Double-sided Si strip detectors (DSSDs) are used as scatterers and CdTe pixel detectors are used as absorbers. In order to increase the efficiency of Compton scattering, the DSSDs are tightly stacked in many layers. The CdTe pixel detectors are arranged around the DSSD stack to detect scattered gamma-rays with high efficiency.

When a gamma-ray photon is scattered in one DSSD and absorbed in one CdTe pixel detector, the incident energy of the gamma-ray and the scattering angle can be determined as

$$E_{\text{in}} = E_1 + E_2 \tag{1}$$

$$\cos\theta = 1 - \frac{m_e c^2}{E_2} + \frac{m_e c^2}{E_1 + E_2} \tag{2}$$

where E_{in} is the incident energy, E_1 is the energy of the recoil electron detected in the DSSD, E_2 is the energy of the

*Corresponding author.
E-mail address: watanabe@astro.isas.jaxa.jp (S. Watanabe).

0168-9002/$ - see front matter © 2007 Elsevier B.V. All rights reserved.
doi:10.1016/j.nima.2007.05.306

scattered photon absorbed by the CdTe and θ is the scattering angle. If one measures the Compton scattering point, recoil electron energy, and scattered gamma-ray energy and position relative to the Compton scattering point, then the energy of the incident gamma-ray is determined, and the direction of the incident gamma-ray lies somewhere on a cone defined by these measurements.

The combination of Si and CdTe is suitable for gamma-rays that range from several tens of keV to a few MeV. The photo-absorption cross-section of Si is small, and the Compton cross-section becomes relatively large because of the small atomic number of Si ($Z = 14$). Additionally, Si works better than other materials with larger atomic numbers in terms of the "Doppler broadening" effect [3].

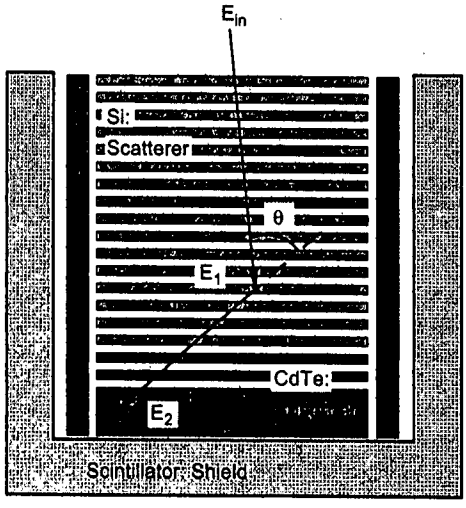

Fig. 1. Schematic picture of our Si/CdTe semiconductor Compton camera.

On the other hand, CdTe has high photo-absorption efficiency for gamma-rays in this energy region, due to their high atomic numbers of 48 and 52.

2. The results from the first prototype of the Si/CdTe Compton camera

We constructed a prototype of the Si/CdTe Compton camera in order to demonstrate the concept described above [4,5]. The prototype consisted of six layers of DSSDs and three CdTe pixel detectors. The DSSD has an area of 2.56 cm × 2.56 cm and a thickness of 300 μm. The strip pitch of the DSSD is 400 μm and each side has 64 strips. The CdTe pixel detector is based on the Schottky CdTe diode device, utilizing indium as the anode and platinum as the cathode [6,7]. The CdTe crystal is manufactured by ACRORAD in Japan using the Traveling Heater Method. The detector has dimensions of 18.55 mm × 18.55 mm and a thickness of 500 μm. The indium side is used as a common electrode. The platinum side is divided into 8 × 8 pixel sections surrounded by a 1 mm wide guard ring. The pixel size is 2 mm × 2 mm, and the gap between the pixels is 50 μm. Each pixel is connected to a fanout board by using In/Au stud bump bonding technology [8]. The signals from the DSSDs and CdTe pixel detectors are processed by low noise analog ASICs, VA32TAs.

By irradiating the prototype with gamma-rays from radio isotopes (^{133}Ba, ^{57}Co, ^{22}Na and ^{137}Cs), we have successfully obtained Compton reconstructed images and spectra from 80 to 662 keV. Fig. 2 shows Compton reconstructed images of ^{133}Ba and ^{22}Na sources obtained with the Compton camera. These images are drawn using conventional Compton reconstruction. First, we select "two-hit events"; that is, one hit to the DSSD and one

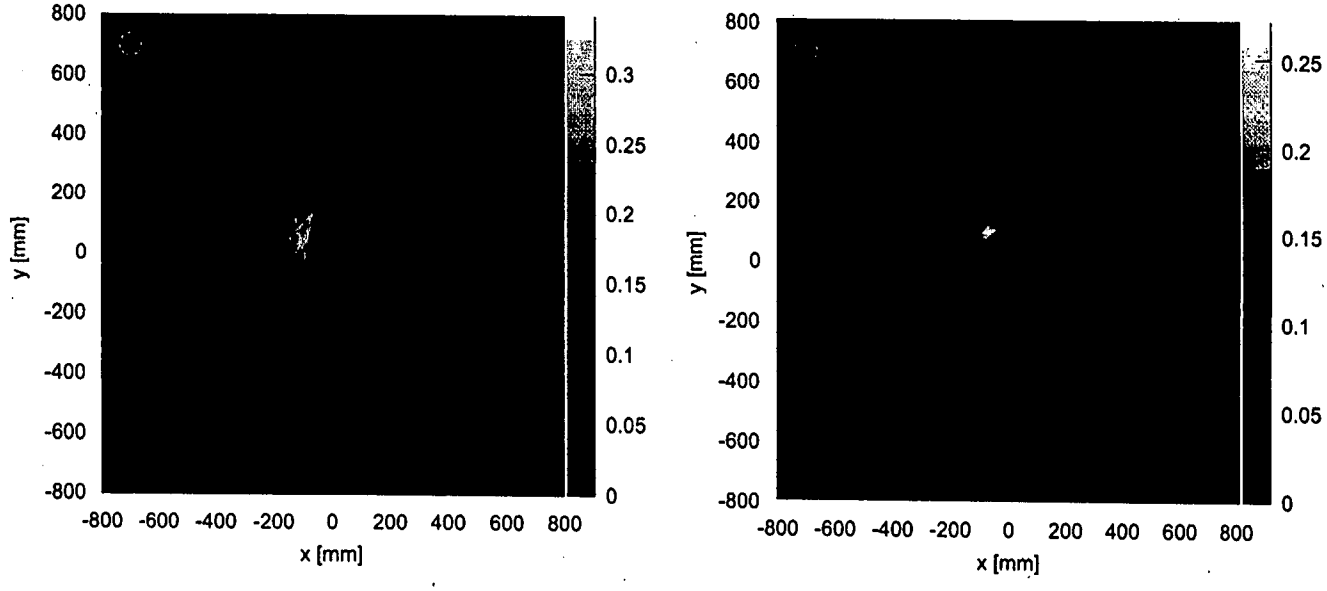

Fig. 2. Compton reconstructed images of 80 keV gamma-rays from ^{133}Ba (left) and 511 keV gamma-rays from ^{22}Na (right). Circles with a radius of 5° are drawn together with the images.

hit to the CdTe. The scatter angle is obtained for each two-hit event. From the scatter angle and the two-hit positions, a Compton cone is drawn on the sky event by event. We then project the cone onto the plane, and obtain the final image.

Due to the good energy resolution of both the DSSDs and the CdTe pixel detectors, good angular resolution was obtained. The achieved angular resolution almost reaches the theoretical limit due to Doppler broadening. Additionally, an important point to note is that the Compton reconstruction for low energy gamma-rays such as 80 keV is achieved. When 80 keV gamma-rays are scattered, the energy of the Compton recoiled electron is only about 10 keV. The achieved energy threshold level is 6 keV for our DSSDs. This is what enabled us to obtain the Compton image for such low energy gamma-rays.

We have established a working model of the Si/CdTe semiconductor Compton camera concept with this prototype. The prototype experiment demonstrates that it is possible to build a Si/CdTe Compton camera that reaches the theoretical limit of angular resolution as a result of Doppler broadening. In response to the prototype results, we have set our goal: Si/CdTe semiconductor Compton cameras with a 1% energy resolution (ΔE(FWHM)/E), the Doppler-limited angular resolution and a 10% detection efficiency. In the following sections, we report our developments of DSSDs and CdTe pixel detectors for the next version of the Compton camera.

3. Development of a new DSSD stack

First of all, in order to improve the efficiency of Compton scattering, a tight stack of DSSDs is necessary. We therefore designed and constructed new DSSD modules to create a compact DSSD stack. Fig. 3 shows pictures of the DSSD module. The size of the DSSD is 2.56 cm × 2.56 cm with a thickness of 300 μm. The strip pitch is 400 μm. Each side has 64 strips and the signals from the strips are processed by new analog ASICs, VA64TAs, which were developed by this research team in conjunction with IDEAS. The VA64TA features low noise performance and low power consumption [5].

The stack pitch of 2 mm is available by using the DSSD modules. For 10% Compton efficiency, 40 layers of 300 μm thick DSSDs or 24 layers of 500 μm thick DSSDs are required [9,10]. It is essential to reduce the gap between the DSSD layers and to stack them tightly. If DSSDs are stacked loosely, the DSSD stack becomes too tall. In this case, too many CdTe detectors are needed to prevent the gamma-ray photons scattered in the DSSDs from escaping.

It is also important to reduce material around the DSSDs for effective detections of low energy (~100 keV) gamma-ray in the Compton camera. The gamma-ray photons scattered in DSSDs must reach an absorber detector directly without being scattered or absorbed. Therefore, we have used kapton plastic as the DSSD jig

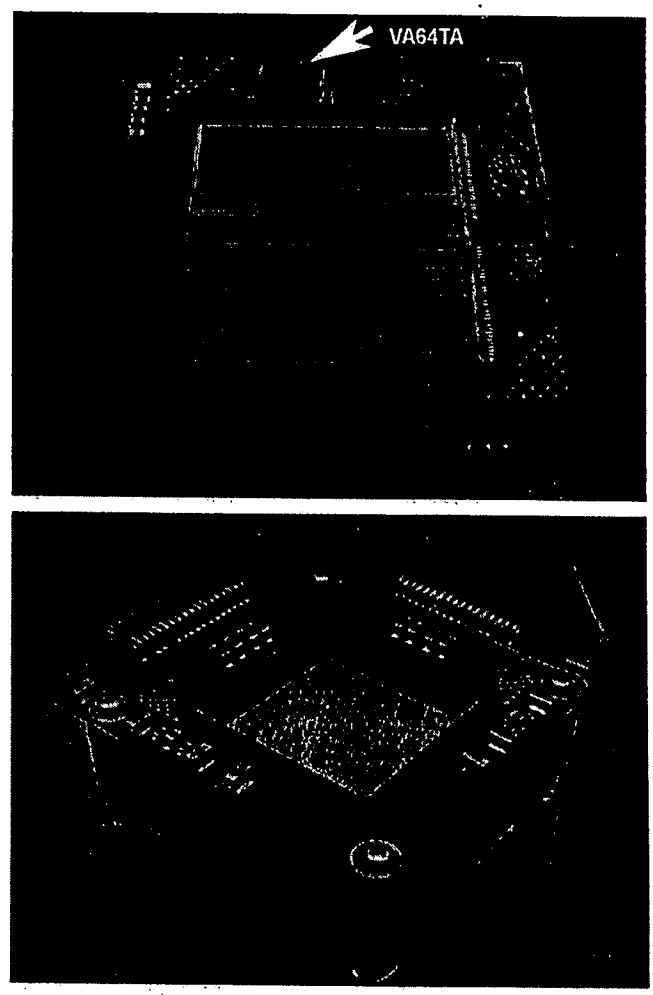

Fig. 3. The new DSSD module and the new DSSD stack. The size of the DSSD is 2.56 cm × 2.56 cm. The 0.3 mm thick DSSDs are stacked in four layers. The pitch between the layers is 2 mm.

material instead of the Al_2O_3 ceramic used in previous modules.

For the first step, we have stacked the DSSD modules in four layers and have tested the DSSD stack in photo-absorption mode by applying a bias voltage of 100 V between the P-side and the N-side. Fig. 4 shows gamma-ray spectra obtained with P-side strips. The average energy resolution from all P-side strips was 1.5 keV (FWHM) at 59.54 keV with an operating temperature of −10 °C. More details about the DSSD modules' properties are described in Takeda et al. [11].

4. CdTe Pixel detector module

In the Si/CdTe Compton camera, CdTe pixel detectors have to cover the DSSD stack with a large solid angle in order to absorb as many gamma-rays scattered in the DSSDs as possible. We designed a CdTe pixel detector module and constructed a number of these modules.

Fig. 5 shows the newly developed CdTe pixel module. The CdTe crystal is manufactured by ACRORAD in Japan

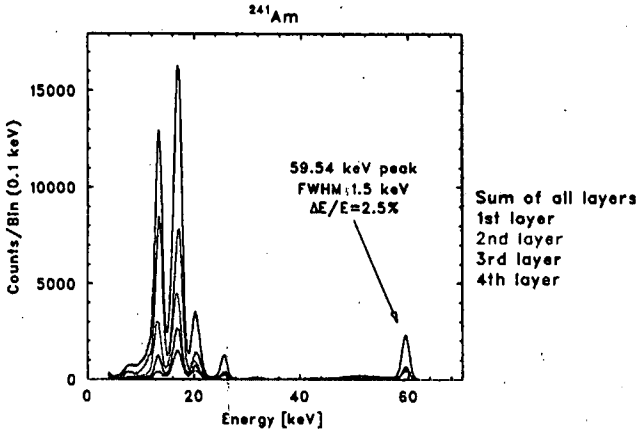

Fig. 4. ^{241}Am spectra obtained with the DSSD stack. The grays show spectra from the first layer, the second layer, the third layer and the fourth layer, respectively. The black spectrum shows the sum of all layers. The achieved energy resolution is 1.5 keV (FWHM) at 59.54 keV. The operating temperature is −10 °C.

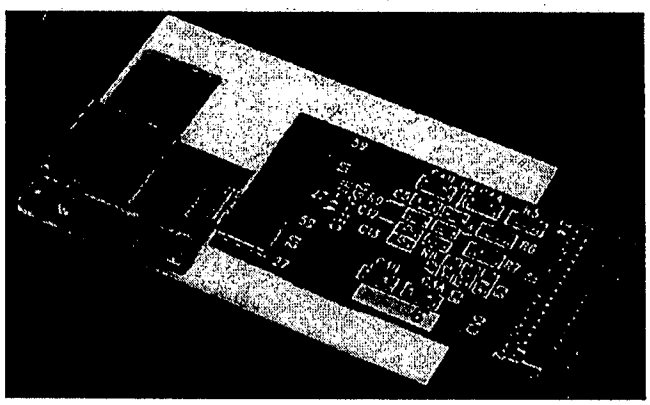

Fig. 5. The newly developed CdTe pixel detector module.

using the Traveling Heater Method. The size of the CdTe device is 13.35 mm × 13.35 mm and the thickness is 0.5 mm. This is a Schottky CdTe diode device, utilizing indium as the anode and platinum as the cathode [6,7,12,13]. The indium side is used as a common electrode, and the platinum side is divided into 8 × 8 = 64 pixels. The pixel size is 1.35 mm × 1.35 mm, and the gap between the pixel electrodes is 50 μm. Around the pixels, a guard ring electrode with a width of 1 mm is attached. This is attached so as to reduce leakage current, as most of the leakage current occurs through the device perimeter [14]. Additionally, a thin layer of gold is evaporated on the Pt side for the purpose of the ensuring good bump bonding connectivity.

In order to connect the pixels to the one-dimensional ASIC, a fanout board was designed. The substrate of the fanout board is made from a 96% Al_2O_3 ceramic with a thickness of 300 μm. The fanout board consists of bump pads, through-holes and patterns that route the signal from bump pads on both surfaces of the ceramic substrate.

Each pixel is connected to the bump pads on the fanout board by In/Au stud bump bonding technology, developed specifically for CdTe detectors [8]. A needle-shaped stud consisting of two stages of gold studs is fixed to the bump pad of the fanout board. The studs are made with a gold wire, and a thin layer of indium is printed on the top of the stud. There are 92 studs, including 64 for the pixels and 28 for the guard ring. The CdTe device and the fanout board are then pressed under controlled temperature conditions. In the previous design of the CdTe pixel detector, epoxy resin was used to fill in the space between the CdTe device and the fanout board. However, we found that epoxy resin degraded electrical resistance properties. Therefore, in this version, no epoxy resin was used. The mechanical strength of the module is still maintained, even without the use of epoxy resin.

Before wire bonding from the fanout board to the ASIC, we measured the leakage current. In our previous study, we found that the leakage current measurements of the detectors assist in the selection of good detectors [15]. The setup of the leakage current measurement is shown in Fig. 6. The sum leakage current of all 64 pixels and that of the guard ring were simultaneously measured separately. By bringing a probe into contact with the through hole on the ceramic fanout board, the pixel electrode side can be accessed without damaging the electrodes. We took the *I-V* curve up to 700 V and the time variation of the leakage current under a bias voltage of 700 V at a temperature of 20 °C. We then performed the selections to build up the pixel modules. The selection criterion is that the leakage current under the bias voltage of 700 V must be stable. This is, any variance must remain within a 10% variation range for a period of two hours.

We measured the leakage currents of 106 bump bonded CdTe devices and selected 74 devices from these. The distribution of the leakage currents for the pixels under a bias voltage of 700 V in a temperature of 20 °C approximated the Landau distribution. The most probable value was 1.2 nA and the sigma was 0.19 nA. Each selected device was wire bonded to a VA64TA. CdTe pixel modules were then created from the selected devices.

We tested the pixel modules by irradiating them with gamma-rays from radio isotopes. Fig. 7 shows ^{241}Am and ^{57}Co spectra obtained from one of the CdTe pixel detector

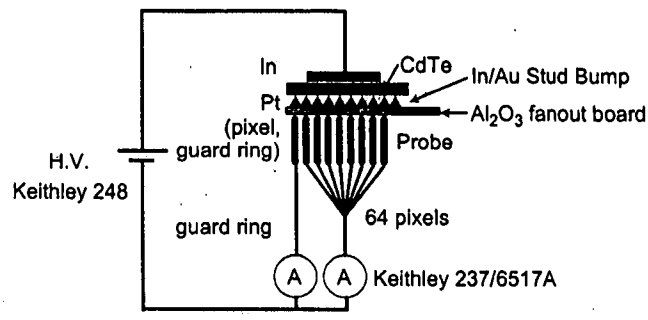

Fig. 6. The setup of the leakage current measurement.

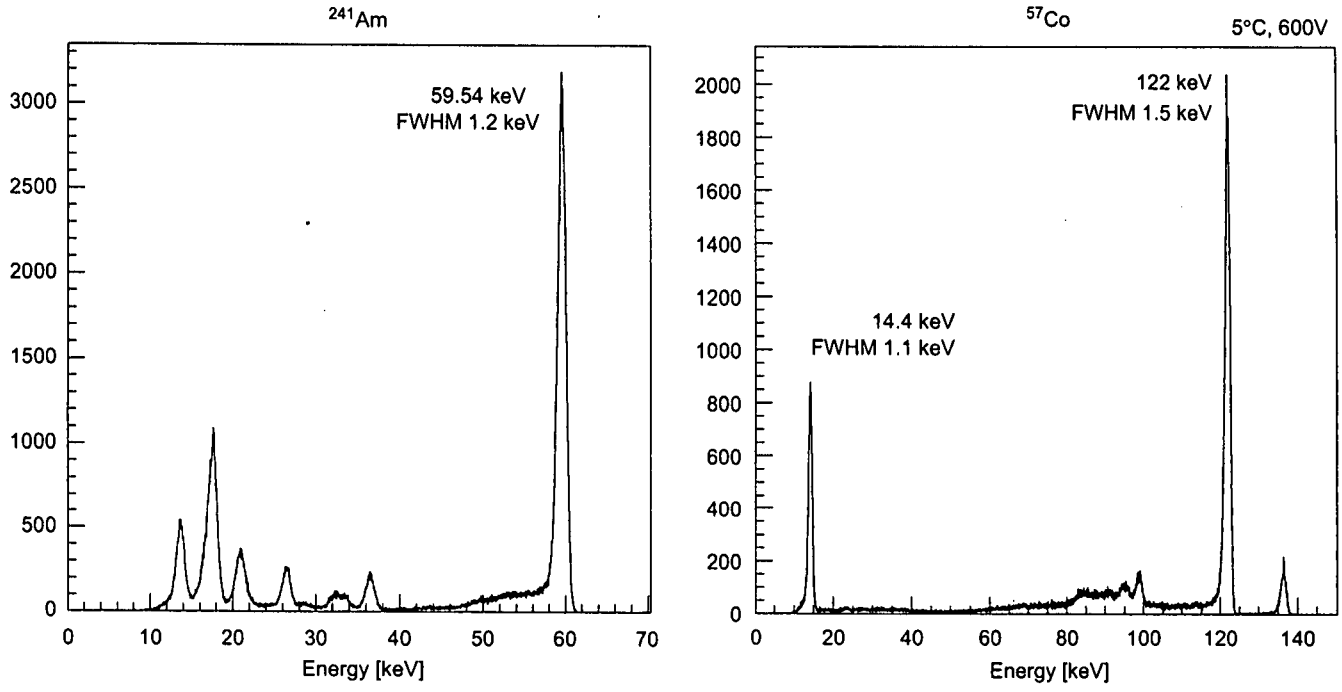

Fig. 7. The ^{241}Am and ^{57}Co spectra obtained from one of the CdTe pixel detector modules. These are summed spectra from all 64 pixels. The applied bias voltage is 600 V, and, the operating temperature is 5 °C. The energy resolutions are 1.2 and 1.5 keV (FWHM) at 59.5 and 122 keV, respectively.

modules. For 64 spectra from all pixels, gain corrections were performed and then all corrected spectra were summed. The applied bias voltage was 600 V and the operating temperature was 5 °C. The energy resolutions were 1.2 and 1.5 keV (FWHM) at 59.5 and 122 keV, respectively. The remarkably close resolution results were achieved for all the pixel modules, using the 74 CdTe devices selected from the leakage current measurement tests mentioned above.

5. CdTe stack detector as the absorber detector for the Compton camera

Stacking a number of thin CdTe detectors is a good way to obtain a high detection efficiency for higher energy gamma-rays. Since the carriers in CdTe have low mobility and a short life time, it is difficult for thick CdTe devices to accomplish full charge collections and high energy resolution. In our previous studies, we demonstrated that both good energy resolution and good detection efficiency can be achieved with the CdTe stack detector. These were achieved using planar CdTe diode detectors with a thickness of 0.5 mm [16–18]. As the absorber detector of the Compton camera, three-dimensional position detection capabilities are necessary in addition to good energy resolution and good detection efficiency. Therefore, in order to build a good absorber detector, we have constructed a CdTe pixel stack detector by stacking the CdTe pixel detector modules.

Fig. 8. The CdTe stack detector. Four layers are stacked. The stack pitch is 2 mm. A layer consists of $2 \times 2 = 4$ CdTe pixel modules.

Fig. 8 shows the stack detector. It has four layers with each layer consisting of the $2 \times 2 = 4$ pixel modules. A stack pitch between layers of 2 mm was attained in this detector.

In order to test performance as an absorber detector, we performed experiments using gamma-rays from radio isotopes. Fig. 9 shows obtained spectra of gamma-rays from ^{133}Ba. Photo-electric absorption peaks are clearly seen in the spectra. The gray lines show the spectra from the first, the second, the third and the fourth layer, respectively. On the low energy side, only the first layer detects gamma-rays. On the other hand, the peak areas

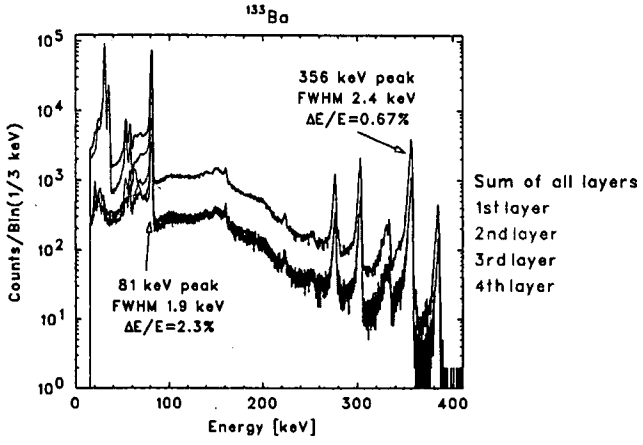

Fig. 9. ^{133}Ba spectra obtained with the CdTe stack detector. The spectrum from each layer is shown in gray, and the summed spectrum of all layers is shown in black. The energy resolutions (FWHM) achieved are 1.9 and 2.4 keV at 81 and 356 keV, respectively.

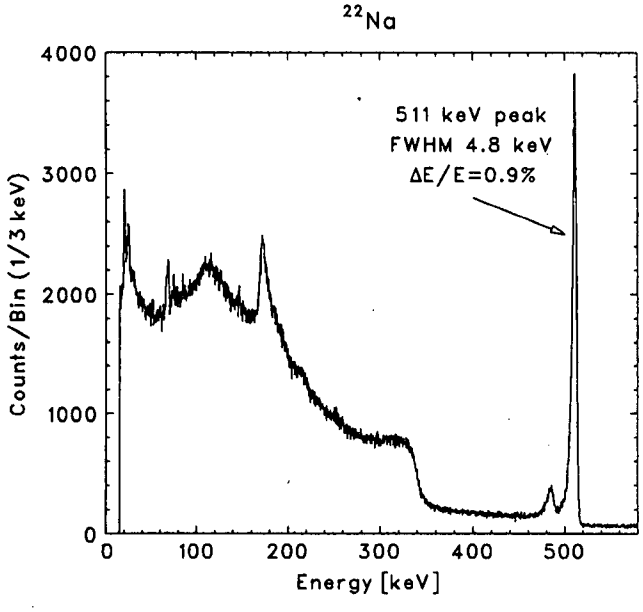

Fig. 10. A 511 keV gamma-ray spectrum obtained with the CdTe stack detector. A ^{22}Na radioisotope is used. The FWHM for 511 keV gamma-ray peak is 4.8 keV ($\Delta E/E$~0.9%).

detected in all layers are almost identical. This shows that the detection efficiency for higher energy gamma-rays was improved by stacking detectors. A 511 keV gamma-ray spectrum obtained with the CdTe stack detector is shown in Fig. 10. The achieved energy resolution is ΔE(FWHM)/E~0.9% at an operating temperature of −20 °C and under the bias voltage of 600 V.

6. Other applications of the CdTe pixel modules

Once CdTe pixel detector modules have been established, they have a variety of applications. One example is a CdTe stack, as discussed in Section 5. This works as a gamma-ray probe with a high energy resolution.

Fig. 11. The large area CdTe imager. The 4 × 4 = 16 CdTe pixel modules are arranged in plates.

Another application is as a large area CdTe imager. By arranging the modules, a CdTe imager with a large area and a high energy resolution can be created. Fig. 11 shows our constructed CdTe imager. The 4 × 4 = 16 CdTe pixel detector modules are arranged on a plate. The total size of the imager is 5.4 cm × 5.4 cm. By attaching a collimator above the image, it works as a conventional gamma camera. Because the imager has a high energy resolution (~1%), various gamma-ray lines can be easily separated in the obtained spectra. Therefore, the imager is capable of simultaneous multi tracer imaging in which different gamma-ray lines are used.

7. Conclusion

We have developed Si and CdTe imaging detectors for the Compton camera. The new four layer DSSD stack and the four layer CdTe pixel detector stack were, respectively, constructed as a scatterer detector and an absorber detector for the Compton camera. The noise performances of the stack detectors was found to be good. With the DSSD stack, we obtained an energy resolution of 1.5 keV (FWHM) for 60 keV gamma-ray photons. For the CdTe pixel detector stack, a $\Delta E/E$~1% energy resolution (FWHM) was achieved. As a next step, we will construct a new Si/CdTe Compton camera using the DSSD stack and the CdTe pixel detector stack.

Acknowledgment

The authors would like to thank C. Baluta for reading the manuscript.

References

[1] T. Takahashi, et al., SPIE 4851 (2003) 1228.
[2] T. Tanaka, et al., SPIE 5501 (2004) 229.
[3] R. Ribberfors, Phys. Rev. B 12 (1975) 2067.

[4] S. Watanabe, et al., IEEE Trans. Nucl. Sci. NS-52 (5) (2005) 2045.
[5] T. Tanaka et al., Nucl. Instr. and Meth. A 568 (2006) 375.
[6] T. Takahashi, et al., Nucl. Instr. and Meth. A 436 (2000) 111.
[7] T. Takahashi, S. Watanabe, IEEE Trans. Nucl. Sci. NS-48 (4) (2001) 950.
[8] T. Takahashi, et al., IEEE Trans. Nucl. Sci. NS-48 (3) (2001) 287.
[9] T. Takahashi, et al., New Astron. Rev. 48 (2004) 309.
[10] H. Odaka, et al., Nucl. Instr. and Meth. A (2007), doi:10.1016/j.nima.2007.05.293.
[11] S. Takeda, et al., Nucl. Instr. and Meth. A (2007), doi:10.1016/j.nima.2007.05.305.
[12] T. Tanaka, et al., New Astron. Rev. 48 (2004) 269.
[13] T. Takahashi, et al., IEEE Trans. Nucl. Sci. NS-49 (2002) 1297.
[14] K. Nakazawa, et al., IEEE Trans. Nucl. Sci. NS-51 (4) (2004) 1881.
[15] S. Watanabe, et al., Nucl. Instr. and Meth. A 567 (2006) 150.
[16] T. Takahashi, B. Paul, K. Hirose, C. Matsumoto, R. Ohno, T. Ozaki, K. Mori, Y. Tomita, Nucl. Instr. and Meth. A 436 (1999) 111.
[17] S. Watanabe, et al., IEEE Trans. Nucl. Sci. NS-49 (3) (2002) 1292.
[18] S. Watanabe, et al., Nucl. Instr. and Meth. A 505 (2003) 118.

Available online at www.sciencedirect.com
ScienceDirect
ELSEVIER
Nuclear Instruments and Methods in Physics Research A 579 (2007) 878–885
NUCLEAR INSTRUMENTS & METHODS IN PHYSICS RESEARCH Section A
www.elsevier.com/locate/nima

Performance study of Si/CdTe semiconductor Compton telescopes with Monte Carlo simulation

Hirokazu Odaka[a,b,*], Shin'ichiro Takeda[a,b], Shin Watanabe[a], Shin-nosuke Ishikawa[a,b], Masayoshi Ushio[a,b], Takaaki Tanaka[a,b], Kazuhiro Nakazawa[a], Tadayuki Takahashi[a,b], Hiroyasu Tajima[c], Yasushi Fukazawa[d]

[a]*Department of High Energy Astrophysics, Institute of Space and Astronautical Science (ISAS), Japan Aerospace Exploration Agency (JAXA), 3-1-1 Yoshinodai, Sagamihara 229-8510, Japan*
[b]*Department of Physics, Graduate School of Science, University of Tokyo, Hongo 7-3-1, Bunkyo 113-0033, Japan*
[c]*Stanford Linear Accelerator Center (SLAC), 2575 Sand Hill Road, Menlo Park, CA 94025, USA*
[d]*Department of Physical Science, Hiroshima University, 1-3-1 Kagamiyama, Higashi-Hiroshima 739-8526, Japan*

Available online 31 May 2007

Abstract

A Compton telescope with high angular resolution and high energy resolution is a promising detector for the next generation of astrophysics space missions aiming at hard X-rays and sub-MeV/MeV gamma-rays. We have been working on a semiconductor Compton camera based on silicon and cadmium telluride (Si/CdTe Compton telescope). The soft gamma-ray detector (SGD) employs a Si/CdTe Compton camera combined with a well-type active shield. It will be mounted on the NeXT mission, proposed to be launched around 2012. One Compton camera module in the SGD will consist of 24 layers of double-sided silicon strip detectors and four layers of CdTe pixel detectors. We carried out Monte Carlo simulations to investigate the basic performance of the detector. Design parameters of devices required in the simulation, such as energy resolution and position resolution of the detector, are based on the results from our prototype detector. From the simulation using current design parameters, the detection efficiency is found to be higher than 10% at ~100 keV and the angular resolution to be 9° and 4.4° at 120 keV and 330 keV, respectively. The effects of changing the design parameters are also discussed.

PACS: 95.55.Ka; 29.40.Wk

Keywords: Gamma-ray detector; Compton telescope; Monte Carlo simulation

1. Introduction

Gamma-rays in the energy range from several tens of keV to several MeV provide an important window to the study of energetic phenomena in the universe such as nucleosynthesis and particle acceleration. These phenomena are observed in objects such as pulsars, stellar black-hole candidates, supernova remnants, active galactic nuclei, and gamma-ray bursts. The observational sensitivity in this energy band, however, is relatively low due to high background levels, low detection efficiency, and limited angular resolution. Compton telescopes are promising detectors to overcome these problems since the direction of incident γ-rays is constrained by Compton kinematics, greatly reducing the background as compared with detectors which employ a coded mask or a collimator.

The first successful Compton telescope in orbit was COMPTEL aboard the Compton gamma-ray observatory (CGRO) [1]. COMPTEL observations provided pioneering results including all sky imaging from 1 to 30 MeV and spectroscopy of MeV gamma-ray lines [2]. But the number of detected objects was very small, with only 32 sources

*Corresponding author. Department of High Energy Astrophysics, Institute of Space and Astronautical Science (ISAS), Japan Aerospace Exploration Agency (JAXA), 3-1-1 Yoshinodai, Sagamihara 229-8510, Japan.
E-mail address: odaka@astro.isas.jaxa.jp (H. Odaka).

0168-9002/$ - see front matter © 2007 Published by Elsevier B.V.
doi:10.1016/j.nima.2007.05.293

detected [3]. Thus improving the sensitivity is the key goal of the next generation detectors. This requires a higher detection efficiency, a lower instrumental background and better angular resolution [4]. A high density detector array with improved energy and position resolution is needed. With this point of view, Compton telescopes based on position-sensitive semiconductor detectors, such as Si, Ge, CZT, and CdTe, have been proposed and developed by various groups [5–10].

Our group has proposed building a Si/CdTe Compton telescope based on the recent achievements of the development of Si and CdTe semiconductor imaging detectors with high energy resolution [9]. A schematic drawing of a Si/CdTe Compton telescope is shown in Fig. 1. The telescope is based on a hybrid semiconductor gamma-ray detector consisting of layers of thin Si and CdTe to detect photons in a wide energy band (0.05–1 MeV). Through using a prototype Compton camera, we succeeded in reconstructing images and spectra of gamma-rays from 81 to 662 keV. We were also able to make photon polarization measurements [11–13].

The Si/CdTe Compton telescope is adopted as one of instruments on board the NeXT (New X-ray Telescope/ Non-thermal Energy eXploration Telescope) mission, proposed in Japan as a successor to the current Suzaku X-ray mission. A detailed description of the instrument, refered to as the SGD (soft gamma-ray detector), is presented in Takahashi et al. [14]. Since the SGD must outperform previous soft γ-ray instruments in background rejection capability, the optimization of the design is of great importance. For this purpose, we have studied the performance of the Si/CdTe Compton telescope by using Monte Carlo simulations. Experimental results of the prototype Compton camera are used for assuming parameters of devices, for example, energy and position resolution of the detector. Initial results of simulations regarding the detection efficiency and performance as a polarimeter were presented in our previous publication [15]. In this paper, we present new results on the performance of the Si/CdTe detector in the SGD. In particular, the detection efficiency as a function of various design parameters and the angular resolution as a function of various data selection are described in detail.

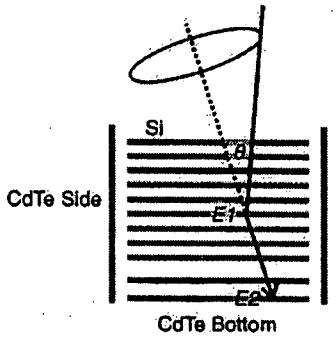

Fig. 1. Schematic picture of a Si/CdTe Compton camera. An incident photon is scattered at a silicon detector and then absorbed at a CdTe detector. E_1 and E_2 are energy deposited of the two hits, and θ is the scatter angle.

2. Simulation Setup

Fig. 2 shows a schematic diagram of the geometry of the detector used in the simulation. The telescope consists of 24 layers of double-sided silicon strip detectors (DSSDs) and four layers of thin CdTe pixellated detectors (CdTe Bottom) with a thickness of 0.5 mm. The sides are also surrounded by CdTe pixel detectors (CdTe Side). In order to lower the background dramatically and thus to improve the sensitivity, we combine a stack of Si strip detectors and CdTe pixel detectors to form a Compton telescope. This configuration is suitable for a Compton camera, since Si has a small cross-section for photo absorption even for very soft γ-rays (e.g. ~80 keV) and CdTe has a large cross-section for photo absorption due to their large atomic numbers ($Z_{Cd} = 48$, $Z_{Te} = 52$). The telescope is then mounted inside the bottom of a well-type active shield to further reduce the background by adopting a new concept, narrow-Field-of-View (FOV) Compton telescope [14,16].

The size of an individual DSSD is 50 mm × 50 mm with a thickness of 0.5 mm, and each DSSD has 125 strips on each side with a strip pitch of 0.4 mm. The energy

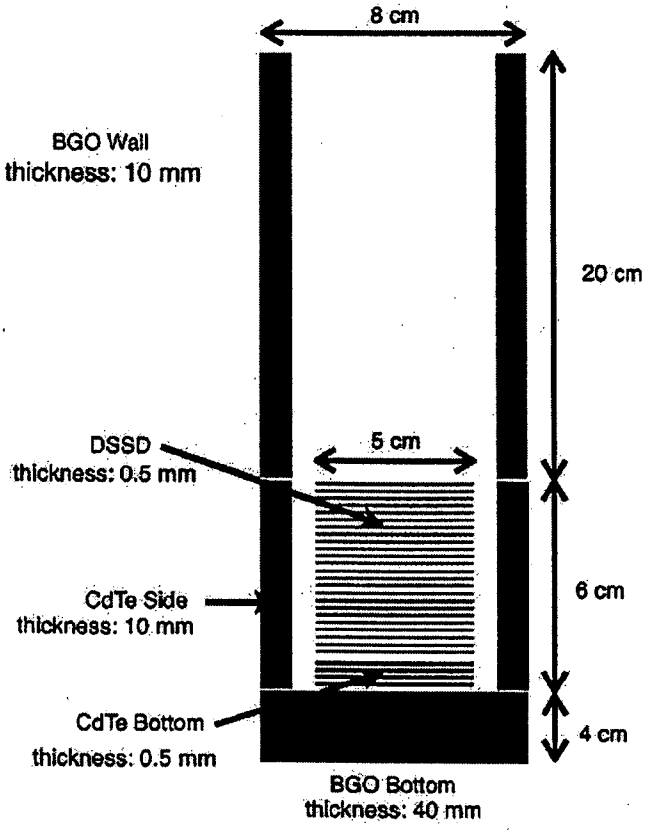

Fig. 2. The simulated geometry of the Si/CdTe Compton telescope.

resolution is assumed to be 1.5 keV (full-width at half-maximum, FWHM), as demonstrated in our previous prototype (also see Ref. [17]). Four layers of CdTe pixel detectors (CdTe Bottom) are also formed as another stack and are placed under the stacked DSSDs. Each CdTe detector consists of 25 × 25 pixels and has a size of 50 mm × 50 mm with a thickness of 0.5 mm. The pixel size is 2 mm × 2 mm. In the simulation, each stack has a frame made of silicon simulating the substrate or electronic devices for data readout, which acts as blocking material around the detector. The thickness is 0.5 mm in the default setting. In addition to these, four CdTe detectors (CdTe Side) cover individual sides of the DSSDs. The thickness of the material associated with the CdTe Side is 10 mm. In the default setting, only the inner 0.5 mm of the CdTe Side is activated as a detector and the rest is used as an anti-coincidence shield. The energy resolution of the CdTe detectors are set at 1.5 keV (FWHM). BGO crystals are placed at both the top and the bottom of the Compton camera. The well-type shield is formed by these crystals along with the outer parts of the 4 CdTe Side detectors. The thickness of the BGO is 10 mm on the side and 40 mm at the bottom.

In the simulation, incident photons have a power-law spectrum with a photon index of −2.1 ranging from 50 to 400 keV, and are generated at the top of the detector, irradiating it uniformly, thus emulating signals from a celestial source. We used the Geant4 simulation toolkit [18] to carry out the simulations and included the G4LECS extension of Kippen [19,20] in order to estimate the effect of Doppler broadening. This broadening is due to the finite momentum of bound electrons in an atom and it results in a deterioration of the angular resolution of Compton telescopes [21].

3. Compton reconstruction

The data taken from the Si/CdTe Compton telescope allow for two analysis modes. The first is the photo absorption mode and the second is the Compton mode. In the photo absorption mode, the energy deposited in all layers is summed if the corresponding deposited energy exceeds a threshold energy of the detector.

In the Compton mode, events satisfying a condition that a photon is scattered once and then absorbed are selected. Once the locations and energies of the two interactions are measured, the Compton equation allows the calculation of the energy and the direction (as a cone in the sky) of the incident γ-ray:

$$E_{\mathrm{in}} = E_1 + E_2 \tag{1}$$

$$\cos\theta = 1 - \frac{m_e c^2}{E_2} + \frac{m_e c^2}{E_1 + E_2} \tag{2}$$

where E_1 is the energy deposited by the Compton scattering and E_2 is that deposited by the photo absorption, m_e is the electron mass and c is the speed of light.

An outline of our Compton reconstruction algorithm is as follows:

(1) Event trigger: The target of analysis is events that have at least one hit which has an energy deposit exceeding the trigger energy of 10 keV. Within the event, all hits that deposited energy exceeding 3 keV are identified and collected.
(2) Clustering: Two hits detected at adjacent pixels or strips are combined into one. The energy deposited is the sum of the two and the newly calculated position is the energy-weighted average of the two hit positions. By this operation, an event such that charge is shared between two adjacent pixels or strips is regarded as one hit.
(3) Anti-coincidence: Events which have at least one hit in the active shield (BGO scintillator and a part of the CdTe Side detector) are rejected. The threshold energy is set at 30 keV.
(4) Two-hit selection: After these screenings, events which have two hits are selected.
(5) "Real Compton" selection: The energy of the recoil electron of Compton scattering E_1 is calculated from the other energy deposited E_2 (assumed to be a photo absorption hit) and the measured scatter angle θ. The value of θ is determined geometrically from the positions of the two hits and the incident direction of the photon, i.e. the FOV of the well-type shield. The significance of the difference between the measured and calculated E_1 is estimated taking account the position resolution, energy resolution, and the effect of the Doppler broadening. Finally, events satisfying the criterion that the calculated E_1 be equal to the measured E_1 within a certain error (4σ) are selected.

It is worth discussing the physics of the identification of the interactions. If a hit takes place at the CdTe Side detectors, we can clearly distinguish between photo absorption and Compton scattering via geometrical considerations. For other hit position combinations, other considerations are needed to identify the order of interactions. In the case of $E_{\mathrm{in}} < m_e c^2/2 = 255$ keV, the energy of the recoil electron by Compton scattering E_1 is always lower than E_2. Thus, the identification is simple. On the other hand, when the incident energy E_{in} exceeds $m_e c^2/2 = 255$ keV, E_1 can be larger than E_2. From the simulation, we found that events such that the photon is scattered at CdTe and then absorbed back at Si ("CdTe Bottom–DSSD" events) are rare. The probability is less than 2% of that of the events of reverse order ("DSSD–CdTe Bottom" events) in the energy band from 255 to 400 keV. Considering this result, we assume that a hit at DSSD is a Compton scattering when one hit is at "DSSD" and the other is at "CdTe Bottom". If two hits take place at the same detector type, "DSSD–DSSD" or "CdTe Bottom–CdTe Bottom" events, we calculate the differences between the measured E_1 and the calculated E_1

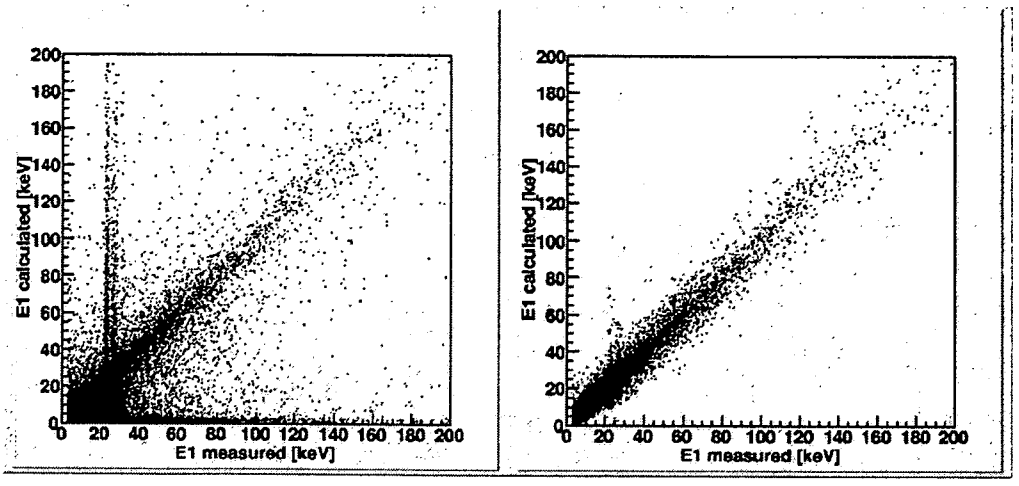

Fig. 3. Comparison of E_1 calculated by Compton reconstruction and actually measured value. The left panel stands for events after the two-hit selection, while the right panel after the "real Compton" selection.

for the two possible orders. We then select the interaction order such that the difference is smaller. By this method, we can determine the "scattering–absorption" order with an accuracy of 99% and 95% for "DSSD–DSSD" and "CdTe Bottom–CdTe Bottom" events, respectively.

Fig. 3 shows the relation between the measured E_1 and the calculated E_1 after the two-hit selection (left) and after the "real Compton" selection (right). In the case of real Compton events, the calculated E_1 is equal to the measured E_1 within the errors. The uncertainty of energy and position measured with the DSSDs and the CdTe pixel detectors contributes to the errors, as does Doppler broadening. After the two-hit selection, there are some bad events such that the calculated E_1 disagrees with the measured E_1. In these events, two hits caused by a fluorescence X-ray emitted from Cd or Te after photo absorption are dominant, being responsible for about 80% of the total of such events. In the left panel of Fig. 3, such events are seen as vertical lines around 20–30 keV. Other sources of error are multiple Compton scatterings or escaped electrons off the detector after photo absorption. Most of the bad events are removed after the "real Compton" selection as shown in the right panel of Fig. 3. For example, more than 90% of the fluorescence X-ray events are rejected by this selection.

4. Detection efficiency

The detection efficiencies in the two different data analysis modes are presented in Fig. 4. For simplicity we hereafter separate the energy band into six bands, 50–70, 70–100, 100–140, 140–200, 200–280, and 280–400 keV. The efficiency of the Compton mode exceeds 10% in the three energy bands below ~120 keV.

Since the Compton camera is composed of DSSDs, CdTe pixel detectors at the bottom (CdTe Bottom), and CdTe pixel detectors at the sides (CdTe Side), we can classify Compton-reconstructed events into six

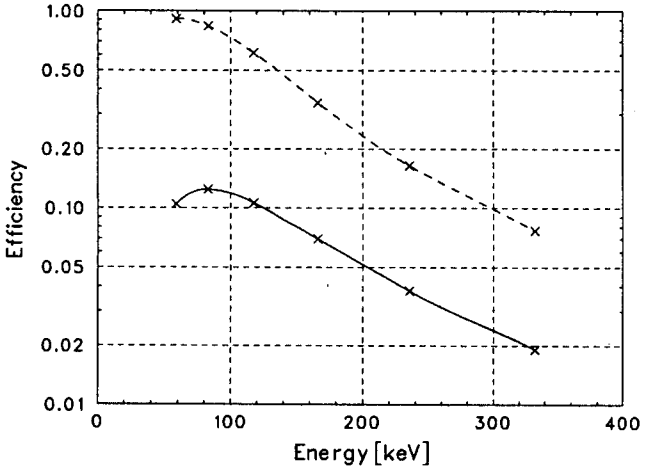

Fig. 4. Detection efficiency of the photo absorption mode (dashed line) and the Compton mode (solid line).

patterns according to their interaction positions, i.e. their detector type. Fig. 5 shows the relative ratio of hit positions of the "scatterring–absorption" events in various energy ranges. The fraction of "DSSD–CdTe Side" events are dominant in all energy bands. Below 100 keV, the probability of "DSSD–DSSD" events is the second highest. As the energy increases, the probability of "DSSD–CdTe Bottom" events or "CdTe Bottom–CdTe Bottom" events increases.

Using the simulations, we evaluated what parameters of the detector design affect the detection efficiency significantly. Fig. 6 shows the detection efficiency as a function of the incident energy for different total thickness of CdTe Bottom detectors. In the default configuration, the total thickness is 2 mm using four layers of CdTe detectors. A thickness of 0.5 mm is sufficient to stop photons below 70 keV. Above 100 keV, setting the total thickness of the CdTe Bottom to 1 mm or greater increases the detection efficiency by a factor of 1.3–1.5.

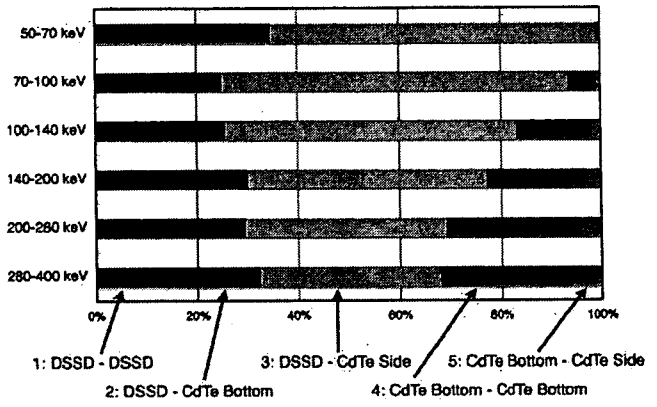

Fig. 5. Relative ratio of hit positions in the six energy bands. 1: "DSSD–DSSD" events, 2: "DSSD–CdTe Bottom" events, 3: "DSSD–CdTe Side" events, 4: "CdTe Bottom–CdTe Bottom" events, and 5: "CdTe Bottom–CdTe Side" events are shown in this order from the left to the right. "CdTe Bottom – DSSD" events are so rare that they cannot be seen in this figure.

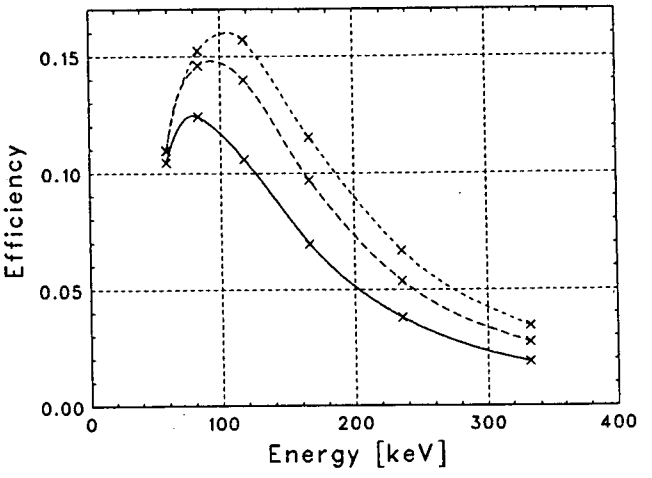

Fig. 7. Detection efficiency in Compton mode with different values of thickness of activated CdTe Side detector; results for 0.5 mm (solid), 1.0 mm (dashed), and 1.5 mm (dotted) are presented.

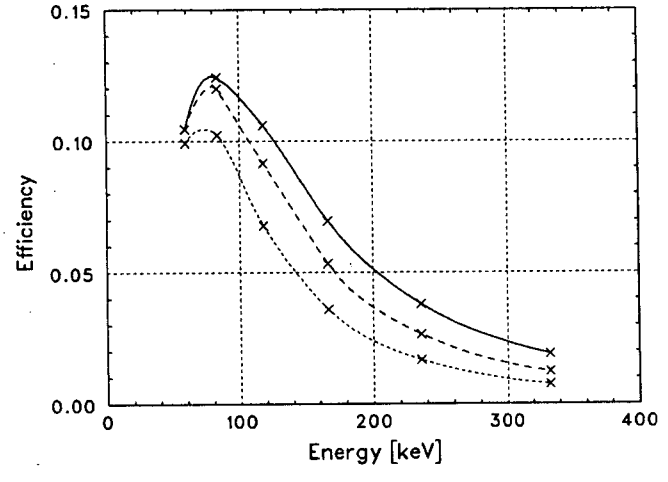

Fig. 6. Detection efficiency in Compton mode with different numbers of activated CdTe Bottom layers; results for four layers (solid), two layers (dashed) and one layer (dotted) are presented. They are equivalent to thickness of 2.0, 1.0, and 0.5 mm, respectively.

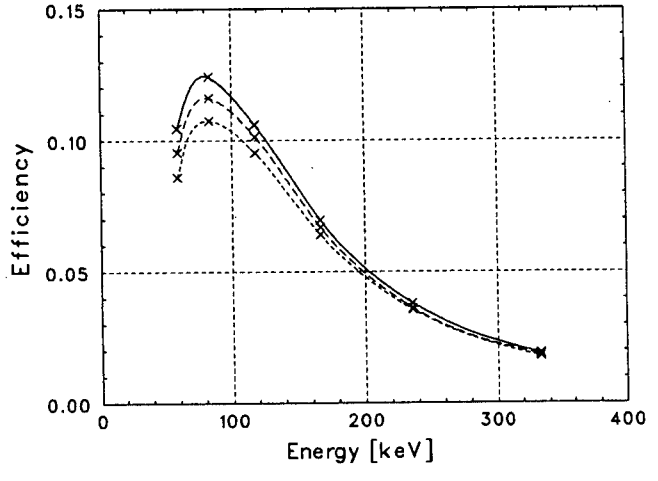

Fig. 8. Detection efficiency in Compton mode for different thickness of Si passive materials around detectors; results with 0.5 mm (solid), 2.0 mm (dashed), and 4.0 mm (dotted) are presented.

Fig. 7 is similar to Fig. 6, but for different total thicknesses of the CdTe Side detectors. The default value is 0.5 mm, which is equivalent to one layer of the CdTe pixel detector employed at the bottom layers. The detection efficiency gets much better as the thickness increases. The efficiency with 1.5 mm thickness exceeds 15% at around 100 keV. Since producing a high resolution CdTe detector thicker than 0.75 mm is technically difficult, increasing the number of layers will be a choice, even though the total number of channels will increase significantly. Adding more CdTe layers at the side improves the detection efficiency better than adding to the bottom for gamma-rays below 300 keV. This result agrees with the large proportion of "DSSD–CdTe Side events" throughout the energy band in this study.

Materials surrounding the detectors, such as substrates and electronic devices for data readout, block photons and decrease the efficiency. The efficiency for several cases of the detector frame thickness is shown in Fig. 8. The material is approximated as pure Si. The effect is not important in the high energy range above a few hundred keV, but is significant below 100 keV.

5. Angular resolution

In this section we evaluate the angular resolution of the Si/CdTe Compton telescope. We define the angular resolution measure (ARM) as $\Delta\theta = \theta_{\text{energy}} - \theta_{\text{geom}}$. Here θ_{energy} is the scatter angle calculated from energy deposits E_1, E_2, and θ_{geom} is that determined from hit positions geometrically. The ARM distributions in the six energy bands are shown in Fig. 9. In this figure, we use only the